Technique for determining the angular orientation of molecules bound to the surface of an arbitrary planar optical waveguide

Sergio B. Mendes, John Thomas Bradshaw, and S. Scott Saavedra

A technique to determine the angular orientation of a molecular assembly bound to the surface of a planar optical waveguide of arbitrary structure is described. The approach is based on measuring the absorption dichroic ratio by using the waveguide evanescent fields with orthogonal polarizations (TE, TM) and the same mode order to probe two molecular assemblies, (i) a reference sample composed of an isotropic orientation distribution of dipoles and (ii) a sample of interest. The isotropic sample is used to characterize the waveguide structure, which then allows the orientation parameters of a molecular assembly under investigation to be determined from a measured dichroic ratio. The method developed here is particularly important for applications in gradient-index and multilayer planar waveguide platforms because in those cases the extension of previously reported approaches would require a full experimental characterization of the guiding structure, which would be problematic and may yield inaccurate results.

OCIS codes: 240.6490, 240.6690, 130.2790, 130.3120.

1. Introduction

Monolayer and submonolayer molecular film assemblies constitute an area of keen interest in many research labs. Because of the potential applications of these assemblies in areas ranging from molecular electronics to bioanalytical sensors, many groups of scientists[1–5] have made a concerted effort to understand the relationship between the orientation of surface-confined molecules and their chemical, physical, and biological properties. Developing a thorough understanding of orientation–function relationships should allow the properties of substrate-supported molecular assemblies to be manipulated to match the requirements of a given application.

Various techniques[6–9] have been employed to study orientation in thin molecular films; they include absorbance linear dichroism measured in a planar optical waveguide geometry, which has the sensitivity required for probing submonolayers of chromophores.[10–13] Mendes and Saavedra[14] have described the determination of orientation parameters from dichroic ratio measurements in planar optical waveguides composed of a single-layer, step-index structure by use of two formalisms: the ray optics model and the electromagnetic wave theory. Both approaches require a complete description of the waveguide structure, which includes the refractive indices of all media (guiding layer, substrate, and cladding media) and the thickness of the guiding layer. Extending these approaches to more-complex waveguide structures, such as gradient-index and multilayer waveguides, is cumbersome. Although the mathematical intricacies could in principle be overcome, the experimental data required are still problematic. For instance, in the case of a gradient-index waveguide a detailed knowledge of the gradient refractive-index profile, which is experimentally difficult to determine with good accuracy,[15] is required. The multilayer waveguide case requires knowledge of the optical constants and thicknesses of all layers. Both types of waveguide are widely used for performing attenuated total reflection measurements of molecular thin films. Because of their ability to easily produce low-loss gradient-index waveguides,[16] ion-exchange techniques have become commonplace for fabricating waveguides of high optical quality. Multilayer waveguides are particularly important because they can provide added functionality to the

The authors are with the Department of Chemistry, University of Arizona, 1306 East University Boulevard, Tucson, Arizona 85721. S. B. Mendes (sergiom@email.arizona.edu) is also with the Optical Sciences Center of the University of Arizona.

Received 6 May 2003; revised manuscript received 7 August 2003; accepted 8 September 2003.

0003-6935/04/010070-09$15.00/0

waveguide structure; one example of such a waveguide is a multilayer electroactive integrated optical waveguide used to perform spectroelectrochemical measurements of submonolayer molecular assemblies.[17,18]

The research presented here provides a straightforward procedure for the determination of orientation parameters that does not require detailed knowledge of the guiding structure and can easily be applied to a variety of waveguide configurations. The procedure involves the measurement of the dichroic ratio in two distinct experiments. First, dichroic ratio ρ, defined as the ratio of the linear absorbance measured at the TE and TM polarizations, $\rho \equiv A_{TE}/A_{TM}$, is measured either for a bulk solution whose absorbing species do not adhere to the waveguide surface (therefore the molecular absorption dipoles are randomly oriented in the bulk phase) or for an adlayer with absorbing dipoles that are isotropically oriented when they are immobilized onto the waveguide surface. The absorbance is measured by use of a guided-wave mode of a particular mode order at the two orthogonal polarizations (TE, TM) to produce a dichroic ratio, ρ_{iso}. Next, in a different experiment with the same waveguide platform, dichroic ratio ρ_{sample} is measured for a molecular adlayer of unknown orientation by use of the same waveguide mode order. These two independent dichroic ratio measurements are used to calculate a normalized dichroic ratio, $\rho_{norm} \equiv \rho_{sample}/\rho_{iso}$. As is shown below, the normalized dichroic ratio can uniquely determine the orientation parameters for the sample under investigation, without any specific information about the structure of the waveguide platform. The derivation below shows that, besides the normalized dichroic ratio, the only information required is the effective refractive index of the guided mode, which can easily be measured from the waveguide coupling condition, and the refractive index of the cladding medium. Applications of the developed approach for an overlayer composed of linear or circular molecular absorption dipoles are considered, and boundary values for the normalized dichroic ratio are established for each type of adsorbed layer. Next, experimental data collected by use of a single-mode step-index solgel glass planar optical waveguide are used to validate the developed theory by comparison of the calculated orientation parameters with those calculated by an approach that requires detailed knowledge of all waveguide parameters.

2. Theory

Let us consider an arbitrary planar optical waveguide structure formed by any number of layers, including gradient refractive-index media, with any number of modes. As a convention, we assume that the waveguide surface is in the x–y plane and that the confined guided modes propagate along the x axis with an effective refractive index N calculated for each polarization and mode order. For each mode order j, the field eigenmodes can be described by

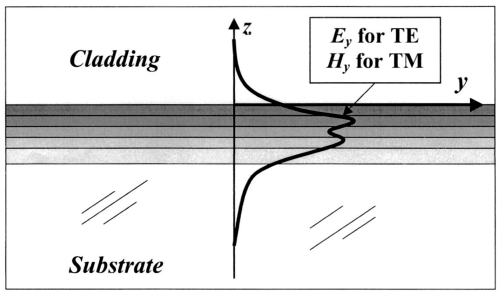

Fig. 1. General waveguide field profile. The field profile represented can be either an electric field $E_y(z)$ for TE modes, or a magnetic field $H_y(z)$ for TM modes. Note that the waveguide surface is chosen in the x–y plane and that the x axis corresponds to the direction of light propagation.

$$\mathbf{E}_j = A_j(z)\exp\left(-i\,\frac{2\pi x}{\lambda}\,N_{TE,j}\right)\exp(i\omega t)\hat{y} \qquad (1)$$

for the transverse electric (TE) polarization and

$$\mathbf{H}_j = B_j(z)\exp\left(-i\,\frac{2\pi x}{\lambda}\,N_{TM,j}\right)\exp(i\omega t)\hat{y} \qquad (2)$$

for the transverse magnetic (TM) polarization. In Eqs. (1) and (2), ω is the angular frequency of the propagating light wave, λ is the vacuum wavelength, t is time, and $\hat{y}$ is a unit vector along the y axis. Figure 1 illustrates a field profile, either E_y or H_y, for a particular mode of an arbitrary waveguide. In general, providing a description of the field profiles, $A_j(z)$ and $B_j(z)$, across the entire waveguide (i.e., for all values of z) can be quite challenging, as it requires complete knowledge of the waveguide structure (refractive index and thickness for each layer, index profile for gradient-index media, or both). However, the evanescent field that decays exponentially away from the waveguide surface into the semi-infinite cladding region ($z > 0$) can easily be described independently of the intricacies of the guiding structure. The exponential decay is determined by the refractive index of the cladding medium, n_c, and the effective refractive index N of the waveguide mode. Mathematically,[19] the field in the cladding region ($z > 0$) is expressed for TE modes by

$$A_j(z) = a_j \exp\left(-\frac{z}{d_{TE,j}}\right), \qquad (3)$$

and for TM modes by

$$B_j(z) = b_j \exp\left(-\frac{z}{d_{TM,j}}\right), \qquad (4)$$

where a_j and b_j are constants that describe the electric and magnetic field amplitudes, respectively, at

the waveguide–cladding interface for each mode j, and d is the field depth in the z direction given by

$$d_{i,j} = \frac{\lambda}{2\pi(N_{i,j}^2 - n_c^2)^{1/2}} \tag{5}$$

for each polarization i = TE or i = TM and mode order j. In the analysis to follow, each mode order j should be treated independently and identically. Hereafter we therefore fix the analysis for a particular mode order and simplify the notation by dropping the symbol j.

For TM modes we use Maxwell's equation, $\nabla \times \mathbf{H} = \partial(\epsilon\mathbf{E})/\partial t$, to obtain expressions for the electric field components, E_x and E_z, in terms of magnetic field H_y:

$$E_x = \frac{-\partial H_y/\partial z}{i\omega\epsilon} = -\frac{i(N_{\mathrm{TM}}^2 - n_c^2)^{1/2}}{\epsilon c} H_y, \tag{6}$$

$$E_z = \frac{\partial H_y/\partial x}{i\omega\epsilon} = -\frac{N_{\mathrm{TM}}}{\epsilon c} H_y, \tag{7}$$

where ϵ is the cladding dielectric constant and c is the vacuum speed of light.

Now we focus on absorbance measurements by using guided wave modes when absorbing species either are uniformly distributed in the cladding medium or form a homogeneous thin layer between the guiding structure and the cladding medium. The absorbance is proportional to the interaction between molecular absorption transition dipole $\boldsymbol{\mu}$ and electric field $\mathbf{E}$ given by $|\boldsymbol{\mu} \cdot \mathbf{E}|^2$. For chromophores dissolved in the cladding region, the electric field components involved in the absorbance calculations are those already given by Eqs. (1), (6), and (7). For a thin (thickness $\ll$ wavelength) layer formed at the waveguide–cladding interface, the in-plane components of the electric field (E_x and E_y) are also those given by Eqs. (1) and (6), as the tangential components of the electric field are continuous across a planar interface. The out-of-plane component of the electric field at the thin layer, $E_{z,l}$, can be derived from the value in the cladding, E_z, given in Eq. (7) by $E_{z,l} = (n_c/n_l)^2 E_z$. In the calculations to follow, we consider $n_c = n_l$ (therefore $E_{z,l} = E_z$), which is a good approximation for molecular films with low surface density at the interface; otherwise the general expression above can easily be carried out through the derivation given below.

The absorbance for each waveguide polarization mode is given by

$$A_{\mathrm{TE}} \propto \int_0^\infty \langle|\mu_y E_y|^2\rangle \mathrm{d}z = \int_0^\infty \langle\mu_y^2\rangle |a|^2 \exp\left(-\frac{2z}{d_{\mathrm{TE}}}\right)\mathrm{d}z \tag{8}$$

for the TE mode and

$$A_{\mathrm{TM}} \propto \int_0^\infty \langle|\mu_x E_x|^2 + |\mu_z E_z|^2\rangle \mathrm{d}z = \int_0^\infty [\langle\mu_x^2\rangle(N_{\mathrm{TM}}^2 - n_c^2) + \langle\mu_z^2\rangle(N_{\mathrm{TM}}^2)] \frac{|b|^2}{(\epsilon c)^2} \exp\left(-\frac{2z}{d_{\mathrm{TM}}}\right)\mathrm{d}z \tag{9}$$

for the TM mode, where $\langle\ \rangle$ denotes an average over an ensemble with a large number of molecules. The previously defined normalized dichroic ratio, ρ_{norm}, can be written as

$$\rho_{\mathrm{norm}} \equiv \frac{\rho_{\mathrm{sample}}}{\rho_{\mathrm{iso}}} = \frac{(A_{\mathrm{TE}}/A_{\mathrm{TM}})_{\mathrm{sample}}}{(A_{\mathrm{TE}}/A_{\mathrm{TM}})_{\mathrm{iso}}}. \tag{10}$$

Substituting the expressions for A_{TE} and A_{TM} given by relations (8) and (9) into the normalized dichroic ratio in Eq. (10) gives us

$$\rho_{\mathrm{norm}} = \frac{\displaystyle\int_0^h \langle\mu_y^2\rangle \exp\left(-\frac{2z}{d_{\mathrm{TE}}}\right)\mathrm{d}z \Big/ \int_0^h [\langle\mu_x^2\rangle(N_{\mathrm{TM}}^2 - n_c^2) + \langle\mu_z^2\rangle N_{\mathrm{TM}}^2] \exp\left(-\frac{2z}{d_{\mathrm{TM}}}\right)\mathrm{d}z}{\displaystyle\int_0^{h_{\mathrm{iso}}} \mu_{\mathrm{iso}}^2 \exp\left(-\frac{2z}{d_{\mathrm{TE}}}\right)\mathrm{d}z \Big/ \int_0^{h_{\mathrm{iso}}} \mu_{\mathrm{iso}}^2 (2N_{\mathrm{TM}}^2 - n_c^2) \exp\left(-\frac{2z}{d_{\mathrm{TM}}}\right)\mathrm{d}z}, \tag{11}$$

where h is the thickness of the sample of interest, h_{iso} is the isotropic sample's thickness (for cladding bulk absorption $h_{\mathrm{iso}} \to \infty$), and μ_{iso} represents the transition dipole for the isotropic system in which all Cartesian components are equal. It is important to note that Eq. (11) has no dependence on the terms a and b that describe the field amplitudes at the cladding–waveguide interface. This result is a direct consequence of our choice to work with the normalized dichroic ratio, as opposed to the sample dichroic ratio. In general, not only may the calculations of field amplitudes at the waveguide–cladding interface require elaborate numerical procedures but they also will certainly require a complete characterization of the waveguide structure, which can be quite problematic for several configurations such as gradient-index and multilayer waveguides. Therefore the addition of an experimental measurement, ρ_{iso}, greatly simplifies the analysis by avoiding complicated numerical procedures and waveguide experimental characterization (e.g., determination of refractive-index profile, thickness, and refractive index of all layers). Equation (11) can be further simplified, as for most cases it can be assumed that $N_{\mathrm{TE}} \approx N_{\mathrm{TM}}$, which makes the

field depths for TE and TM modes approximately equal ($d_{TE} \approx d_{TM}$), giving us

$$\rho_{norm} = (2N_{TM}^2 - n_c^2) \times \frac{\int_0^h \langle \mu_y^2 \rangle \exp\left(-\frac{2z}{d_{TE}}\right) dz}{\int_0^h [\langle \mu_x^2 \rangle (N_{TM}^2 - n_c^2) + \langle \mu_z^2 \rangle N_{TM}^2] \exp\left(-\frac{2z}{d_{TM}}\right) dz}. \quad (12)$$

When $N_{TE} \approx N_{TM}$ may not be considered a good approximation (e.g., for highly birefringent waveguides), it is straightforward to show that Eq. (12) will still hold as long as the isotropic dichroic ratio ρ_{iso} is measured with an isotropic film whose thickness h_{iso} is much smaller than the penetration depth of the evanescent field. We can simplify Eq. (12) further by noting that, for a molecular monolayer, the film thickness is much less than the evanescent depth of penetration, $h \ll d_{TE,TM}$, which gives us

$$\rho_{norm} = \frac{\langle \mu_y^2 \rangle (2N_{TM}^2 - n_c^2)}{\langle \mu_x^2 \rangle (N_{TM}^2 - n_c^2) + \langle \mu_z^2 \rangle N_{TM}^2}. \quad (13)$$

Equation (13) clearly shows that the determination of the normalized dichroic ratio is independent of the waveguide structure. The only required parameters are the waveguide's effective refractive index for the TM mode, N_{TM}, and the index of refraction of the cladding medium, n_c. Next we apply Eq. (13) to an important specific case: An immobilized film that has in-plane symmetry because molecules are randomly oriented in the x–y (waveguide surface) plane. In this case the absorption dipole components can be described by

$$\langle \mu_x^2 \rangle = \langle \mu_y^2 \rangle = \langle \mu_{in}^2 \rangle, \quad (14)$$

$$\langle \mu_z^2 \rangle = \langle \mu_{out}^2 \rangle, \quad (15)$$

$$2\langle \mu_{in}^2 \rangle + \langle \mu_{out}^2 \rangle = \mu^2, \quad (16)$$

where μ_{in} and μ_{out} are, respectively, the in- and out-of-plane Cartesian components of the absorption dipole, whose strength is given by μ. Under the in-plane symmetry assumption, Eq. (13) can be used to determine the range of possible values for the normalized dichroic ratio. The results are summarized in Table 1, where $\langle \mu_{out}^2 \rangle / \mu^2$ spanning the physically acceptable domain {0, 1} is used as an independent variable with which to calculate $\langle \mu_{in}^2 \rangle / \mu^2$ [through Eq. (16)] and ρ_{norm} [through Eq. (13)]. The normalized dichroic ratio spans the range $0 \le \rho_{norm} \le (2N_{TM}^2 - n_c^2)/(N_{TM}^2 - n_c^2)$, and an experimental result outside this region is not consistent with previous assumptions. Furthermore, we can apply the results of Table 1 for a molecular layer composed of either linearly polarized absorption dipoles or circularly polarized absorption dipoles. For a molecular assembly composed of linear dipoles, where θ is defined as the angle between the absorption dipole and the waveguide surface normal (z axis), we have the following expressions for the absorption dipole components:

Table 1. Range of Values for the Normalized Dichroic Ratio

$\frac{\langle \mu_{out}^2 \rangle}{\mu^2}$	$\frac{\langle \mu_{in}^2 \rangle}{\mu^2}$	ρ_{norm}
0	1/2	$\frac{2N_{TM}^2 - n_c^2}{N_{TM}^2 - n_c^2}$
1/3	1/3	1
1/2	1/4	$\frac{2N_{TM}^2 - n_c^2}{3N_{TM}^2 - n_c^2}$
1	0	0

$$\frac{\langle \mu_{in}^2 \rangle}{\mu^2} = \frac{1}{2} \langle \sin^2 \theta \rangle, \quad (17)$$

$$\frac{\langle \mu_{out}^2 \rangle}{\mu^2} = \langle \cos^2 \theta \rangle. \quad (18)$$

As $0 \le \langle \mu_{out}^2 \rangle / \mu^2 \le 1$, the normalized dichroic ratio can span the entire range listed in Table 1. The measurement of the normalized dichroic ratio will uniquely determine the orientation parameter for the molecular assembly through Eqs. (13)–(18). For a molecular layer composed of circularly polarized dipoles, where θ is defined as the angle between the normal to the circular dipole plane and the waveguide surface normal (z axis), we have the following expressions for the absorption dipole components:

$$\frac{\langle \mu_{in}^2 \rangle}{\mu^2} = \frac{1}{4} (1 + \langle \cos^2 \theta \rangle), \quad (19)$$

$$\frac{\langle \mu_{out}^2 \rangle}{\mu^2} = \frac{1}{2} \langle \sin^2 \theta \rangle. \quad (20)$$

Therefore, for an adlayer of circularly polarized dipoles, the in- and out-of-plane dipole components span a smaller range (for example, $0 \le \langle \mu_{out}^2 \rangle / \mu^2 \le 1/2$), and the normalized dichroic ratio is limited to the range $(2N_{TM}^2 - n_c^2)/(3N_{TM}^2 - n_c^2) \le \rho_{norm} \le (2N_{TM}^2 - n_c^2)/(N_{TM}^2 - n_c^2)$. Again, measurement of the normalized dichroic ratio can be used to determine the molecular orientation parameter of the thin film under investigation through Eqs. (13)–(16), (19), and (20).

3. Experiment

A. Integrated Optical Waveguide Spectrometer

An experimental demonstration of the aforementioned theory was performed by use of a broadband planar waveguide spectrometer, which is shown schematically in Fig. 2 and has been described in detail elsewhere.[20] Briefly, this attenuated total reflection (ATR) spectrometer includes a planar integrated optical waveguide (IOW) fabricated by dip coating a

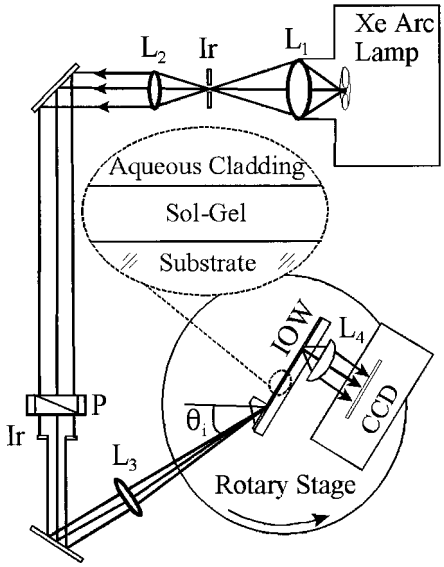

Fig. 2. Optical setup for performing broadband IOW–ATR spectroscopic experiments. The beam path through the optical components is as follows: L_1, 48-cm effective-focal-length (efl) lens; Ir = Iris; L_2, 8-cm efl lens; P, Glan–Taylor prism polarizer; Ir, iris; L_3, 43-cm efl lens. The light is focused into the SF6 prism coupling corner, coupled into the solgel waveguiding layer, and outcoupled through the glass substrate by a surface-relief grating (grating period, 362 nm). The outcoupled light is collimated with 33-mm efl cylindrical lens L_4 onto a CCD camera placed at the lens's back focal plane. Incoupler-to-outcoupler distance for the experiments reported herein, 10 mm.

solgel layer onto a soda lime glass substrate.[21] This waveguide layer was found to support only TE_0 and TM_0 modes for all wavelengths in the range 454.5–632.8 nm. A truncated right-angle (45°–45°–90°) Schott glass prism (SF6) mounted in a Plexiglass flow cell was used as the incoupling element. A white-light source (150-W xenon arc lamp) was spatially filtered, collimated, and polarized by a Glan–Taylor prism before being focused onto the hypotenuse face of the incoupling prism. The prism–waveguide gap was filled with a 50-mM, pH 7, sodium phosphate buffer solution, and pressure was applied to the top of the prism to achieve optimal coupling.[22] By placing the IOW element on a rotary stage we adjusted the spectrometer throughput by setting the angle between the Xe source beam and the incoupling prism to optimize the response for both TE_0 and TM_0 polarization in the region 520–570 nm, as this spectral region encompasses the absorption bands of both types of molecular film used in this study (*vide infra*). An integral surface-relief diffraction grating fabricated into the glass substrate before solgel deposition acted as the dispersive outcoupling element. The grating was fabricated by development of a holographic photoresist pattern followed by reactive ion etching of the grating into the glass substrate, as previously described.[20,23] We determined grating period Λ to be 0.362 μm by measuring the diffraction angle at the Littrow configuration. The light beam outcoupled by the diffraction grating was collected with a 33-mm effective-focal-length cylindrical lens and directed onto a thermoelectrically cooled CCD camera located at the lens's Fourier plane. The solgel waveguide surface used for all experiments reported here was cleaned before experimentation in accordance with previously described procedures.[20]

B. Molecular Films

1. *Isotropic*

For the measurement of the isotropic dichroic ratio, a thin layer of randomly oriented molecules immobilized at the waveguide–aqueous cladding interface was used. This layer consisted of an adsorbed film of dextran labeled with Rhodamine B (Rh-B) dye (40,000 MW; Molecular Probes D-1840). According to the supplier, this material (Rh-B dextran) is synthesized by random labeling of amino dextran with Rhodamine B (5.7 mol/mol of dextran), followed by capping of unreacted amines, which generates a zwitterionic, labeled dextran.[24] Rh-B dextran was chosen to create an isotropic molecular film because of the lack of organized secondary and tertiary structure in dextrans and because of the random nature of the Rh-B labeling process. A reasonable assumption is that adsorption of Rh-B dextran onto a glass waveguide surface does not create a macroscopically ordered structure. Furthermore, because 5.7 mol of Rh-B are randomly conjugated to each mole of dextran, it is also reasonable to assume that the Rh-B absorption dipoles are isotropically oriented in the adsorbed film. The isotropic assumption for the Rh-B dextran film was independently tested and is corroborated in Subsection 4.C below.

2. *Anisotropic*

The molecular layer chosen to be investigated as an ordered sample consisted of 1,1′-dioctadecyl-3,3,3′,3′-tetramethylindocarbocyanine perchlorate (DiI; Molecular Probes D-282) dispersed in a lipid bilayer composed of 1,2-dioleoyl-*sn*-glycero-3-phosphocholine (DOPC; Avanti Polar Lipids 850375). The molecular orientation properties of DiI incorporated into Langmuir–Blodgett films of arachidic acid deposited onto the surface of planar solgel waveguides were investigated previously.[11] The dipoles of the incorporated DiI were found to be oriented at a mean angle of 75° from the normal of the waveguide surface plane. DiI incorporated into a DOPC bilayer should be similarly oriented and thus was selected for examination in this study.

Lipid dispersion was prepared by vacuum evaporation of solvent from a mixture of 0.15 mol % DiI in DOPC dissolved in chloroform. The DiI–DOPC mixture was then resuspended in a 50-mM pH 7 sodium phosphate buffer to a final DOPC concentration of 0.6 mM. A freeze–thaw process, followed by repeated extrusion through a 50-nm polycarbonate filter (Whatman), produced unilamellar lipid bilayer vesicles.[25,26] Vesicle fusion (see below) was used to form bilayers of DiI–DOPC upon planar waveguide surfaces.

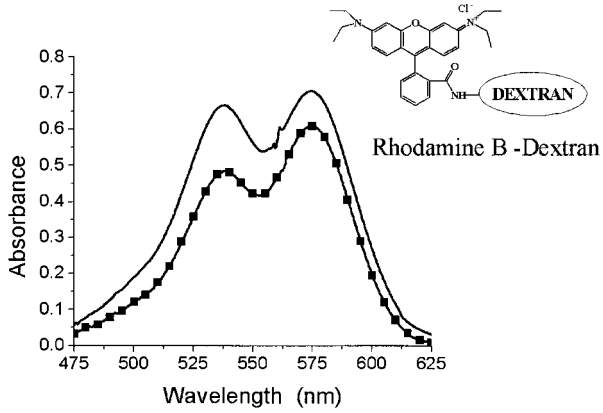

Fig. 3. Experimental IOW–ATR spectra of a film of Rh-B dextran adsorbed onto the surface of a solgel glass waveguide: absorbance spectra for TE_0 (filled squares) and TM_0 (solid curve) polarization.

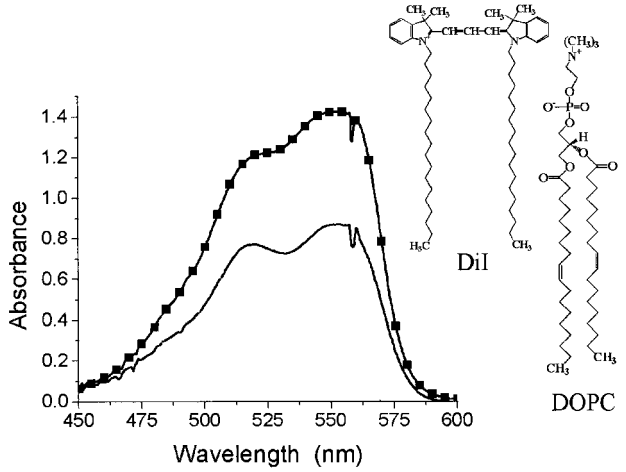

Fig. 4. Experimental IOW–ATR spectra of DiI incorporated into a DOPC lipid bilayer deposited by vesicle fusion onto the surface of a solgel glass waveguide: absorbance spectra for TE_0 (filled squares) and TM_0 (solid curve) polarization.

4. Results and Discussion

A. Polarized Spectral Response

To form an isotropic film adsorbed onto a planar waveguide surface we injected a 6-μM solution of Rh-B dextran in a 50-mM pH 7 sodium phosphate buffer into the waveguide flow cell and allowed it to incubate for 15 min. The cell was then flushed with a 50-mM pH 7 sodium phosphate buffer solution to remove nonadsorbed material, and the spectral intensity (I) in both TE_0 and TM_0 waveguide modes was collected. A blank spectrum with the flow cell filled with only buffer was recorded previously (I_0) for each polarization mode, and the measured absorbance spectra, $A \equiv -\log_{10}(I/I_0)$, are plotted in Fig. 3. The absorbance in the TM_0 polarization is higher than in the TE_0 polarization. Inasmuch as the Rh-B dipoles in the dextran film are assumed to be isotropically oriented, the difference in absorbance intensity is attributed to differences in the effective TE_0 and TM_0 path lengths for the particular waveguide structure employed in this experiment.

To form an anisotropic film adsorbed to a planar waveguide surface we injected the 0.6-mM DiI–DOPC vesicle solution into the waveguide flow cell and incubated it for ~10 min. During this period, a waveguide-supported lipid bilayer was formed by vesicle fusion and spreading.[27–29] The flow cell was then flushed with buffer solution to remove any nonfused vesicles, and the TE_0 and TM_0 polarized spectra were collected. The absorbance spectra are plotted in Fig. 4, which displays a significantly stronger absorbance in TE_0 than in TM_0, the opposite of the data obtained on the isotropic film (Fig. 3). Because the DiI molecular dipole is thought to be oriented in the plane of the lipid bilayer,[11] its dichroic ratio is expected to be higher than in the isotropic case. However, there are two effects that contribute to the difference between the TE and the TM spectra: an anisotropic orientation distribution of DiI molecules and waveguide path-length differences between the two polarizations. The sample dichroic ratio, $\rho_{sample} = A_{TE,sample}/A_{TM,sample}$, incorporates both effects. As shown above, the normalized dichroic ratio, ρ_{norm}, factors out the path-length difference and provides a clear quantification of the dichroism that is due solely to the anisotropic molecular orientation.

We used the polarized spectra acquired for the isotropic Rh-B dextran film (Fig. 3) to calculate the isotropic dichroic ratio, $\rho_{iso}(\lambda)$, at each wavelength in the 480–580-nm spectral window, which is the window that was used for all the calculations given below. The corresponding dichroic ratio at each wavelength for the anisotropic DiI–DOPC film, $\rho_{sample}(\lambda)$, was obtained from the polarized spectra shown in Fig. 4. Combining these two results provided us the normalized dichroic ratio $\rho_{norm}(\lambda)$ over the spectral window of analysis.

B. Molecular Orientation

Proceeding with the method described herein, we determined the effective refractive index of the waveguide structure for the TM_0 mode, N_{TM}, and the refractive index of the cladding medium, n_c. We determined N_{TM} by measuring the incident angle of a light beam impinging upon a grating coupler that resulted in a bound TM_0 mode. This measurement was performed at several wavelengths produced by an Ar^+-ion laser with the waveguide flow cell filled with the same cladding solution (50-mM phosphate buffer) that was used in the dichroic ratio measurements. A polynomial fit to the data was used to generate a dispersion curve approximated by $N_{TM} = 1.473 + 18{,}000\ \text{nm}^2/\lambda^2$. The optical dispersion of the cladding (buffer solution) was estimated from tabulated values for the refractive index of water[30] with a Cauchy fit given by $n_c = 1.32384 + 3117\ \text{nm}^2/\lambda^2$.

A planar supported lipid bilayer composed of DOPC doped with DiI is expected to have in-plane symmetry because of its molecular structure.

Therefore we can use Eqs. (13)–(16) to solve for the in- and out-of-plane dipole moments, yielding

$$\frac{\langle \mu_{in}^2 \rangle}{\mu^2} = \frac{1}{2} - \frac{\langle \mu_{out}^2 \rangle}{2\mu^2} = \frac{\rho_{norm} N_{TM}^2}{(2N_{TM}^2 - n_c^2) + \rho_{norm}(N_{TM}^2 + n_c^2)}. \quad (21)$$

We then used the measured values for ρ_{norm}, N_{TM}, and n_c at each wavelength (292 points equally spaced in the 480–580-nm spectral region) to calculate $\langle \mu_{in}^2 \rangle/\mu^2$ and $\langle \mu_{out}^2 \rangle/\mu^2$. An average value and a standard deviation were calculated over the specified wavelength range with the following results: $\langle \mu_{in}^2 \rangle/\mu^2 = 0.44 \pm 0.01$ and $\langle \mu_{out}^2 \rangle/\mu^2 = 0.13 \pm 0.03$. As $\langle \mu_{in}^2 \rangle/\langle \mu_{out}^2 \rangle = 3.4$, the molecular absorption dipoles show a preferred orientation toward the film plane. In the next step, we determined a mean orientation angle $\bar{\theta}$ by invoking the commonly used assumption of a delta function for the molecular orientation distribution. Because the DiI molecule in DOPC can be considered an ensemble of linear absorption dipoles, the mean angle can be solved by either Eq. (17) or (18) by use of the calculated values for $\langle \mu_{in}^2 \rangle/\mu^2$ or $\langle \mu_{out}^2 \rangle/\mu^2$, respectively. The result, $\bar{\theta} = 69° \pm 2°$, agrees well with previously published results[11] of $\bar{\theta} = 75° \pm 4°$ for DiI doped into an arachidic acid film deposited by the Langmuir–Blodgett technique. The small difference in mean tilt angle between DiI dispersed in DOPC and arachidic acid films is likely due to differences in film structure and film deposition techniques.[9,31]

It is important to emphasize that the information required for determining the absorption dipole components and the mean orientation angle were composed of (a) the measured dichroic ratio of the sample under investigation (DiI–DOPC), (b) the measured dichroic ratio of a randomly oriented film (Rh-B dextran), (c) measurement of the waveguide's effective refractive index N_{TM}, and (d) the refractive index of the cladding medium, n_c. All these parameters are obtainable by relatively simple experimental measurements. Considering that the theoretical derivation described in Section 2 is general, meaning that it does not assume a particular waveguide structure, the new approach presented here provides a straightforward and simple procedure with which to treat more-complex guiding configurations such as gradient-index and multilayer waveguides for similar studies of molecular film orientation.

As a final note, we point out the utility of the broadband solgel IOW spectrometer for measuring dichroism in molecular films. The ability to measure broadband spectra allows dichroic parameters to be calculated over a broad spectral range. Averaging the dichroic response over a molecular absorption band reduces the likelihood that artifacts associated with performing measurements at single wavelengths will produce erroneous results.

C. Comparison with an Existing Method

It is interesting to compare the results obtained from the new approach presented above with those obtained by use of an approach previously applied[14] to determine molecular orientation in films deposited onto single-layer step-index waveguides. The earlier approach requires full characterization of the waveguide structure, including the refractive index and the thickness of the guiding layer (n_{wg} and t_{wg}), the refractive indices of the cladding (n_c) and the substrate (n_s) media, and the waveguide's effective refractive index at both polarizations, N_{TE} and N_{TM}. For a single-layer step-index waveguide these quantities can be determined with good accuracy. Because this simple waveguide structure was also used to test the new approach, a comparison of the two approaches for extraction of molecular orientation information can be made. As described in Ref. 14, the dichroic ratio for a single-layer step index waveguide is given by

$$\rho_{sample} = \frac{\langle \mu_{in}^2 \rangle (n_{wg}^2 - N_{TE}^2)}{N_{TE}(n_{wg}^2 - n_c^2)} \frac{N_{TM}[n_{wg}^4(N_{TM}^2 - n_c^2) + n_c^4(n_{wg}^2 - N_{TM}^2)]}{n_{wg}^2(n_{wg}^2 - N_{TM}^2)\left[(N_{TM}^2 - n_c^2)\langle \mu_{in}^2 \rangle + \left(\frac{n_c}{n_l}\right)^4 N_{TM}^2 \langle \mu_{out}^2 \rangle\right]} \frac{t_{eff,TM}}{t_{eff,TE}}, \quad (22)$$

where $t_{eff,TE(TM)}$ is the waveguide's effective thickness for the TE (TM) mode. The effective refractive index for the TE mode, N_{TE}, of the solgel waveguide was determined to follow a dispersion curve fitted by $N_{TE} = 1.473 + 20{,}700\ \text{nm}^2/\lambda^2$ (measured by use of the grating coupling condition as described above). We used the effective refractive indices, N_{TE} and N_{TM}, in both polarizations to determine the optical properties (n_{wg}, t_{wg}) of the solgel waveguide layer, which displayed a dispersion curve approximated by $n_{wg} = 1.53 + 25{,}000\ \text{nm}^2/\lambda^2$ and a thickness of 250 nm. The refractive index for the soda lime glass substrate, n_s, used for determination of $t_{eff,TE(TM)}$ was approximated by $n_s = 1.51$, and we used the approximation $n_c = n_l$. All remaining parameters in Eq. (22) were as stated above. Using the polarized absorbance spectra for the DiI/DOPC film (Fig. 4), we solved Eq. (22) for the molecular dipole components, assuming in-plane symmetry, as described above. The calculated average value for the in-plane component was $\langle \mu_{in}^2 \rangle/\mu^2 = 0.435 \pm 0.005$, from which an average tilt angle of $\bar{\theta} = 68.9° \pm 0.8°$ was calculated. These values for $\langle \mu_{in}^2 \rangle/\mu^2$ and $\bar{\theta}$ agree well with those

calculated by the new approach. Consistency with the previous approach further establishes the validity of the new approach.

Finally, we emphasize an important point regarding implementation of the new approach. A truly isotropic molecular ensemble must be characterized on the same waveguide platform that is used for measurement of the film of unknown (but presumably anisotropic) structure. Here, the use of the single-layer step-index waveguide platform described by Eq. (22) is useful for assessing whether a molecular film satisfies the isotropic requirement. Using the polarized spectra for Rh-B dextran film shown in Fig. 3 and solving Eq. (22), we calculated a value of $\langle \mu_{in}^2 \rangle / \mu^2 = 0.33 \pm 0.01$. This value agrees well with the theoretically predicted value of 1/3 for a truly isotropic film. These results validate the assumption of an isotropic orientation distribution for an adsorbed Rh-B dextran film and therefore make the procedure described here a useful test system for characterizing path-length differences between TE and TM modes in an arbitrary waveguide structure.

5. Conclusions

We have developed a straightforward, simple procedure for determining mean angular orientation in thin-film molecular assemblies deposited onto the surface of a planar optical waveguide of arbitrary structure. Planar optical waveguides of any number of layers, including gradient-refractive-index media, and any number of modes can be treated by the method presented here. This approach overcomes previous difficulties in the application of many important waveguide platforms to studies of molecular orientation in surface-immobilized assemblies.

This paper is based on research partially supported by the National Science Foundation under grant CHE-0108805 to S. S. Saavedra. We gratefully acknowledge assistance from Eric Ross in the production of unilamellar vesicles and a helpful discussion with Wally Doherty.

References and Notes

1. J. D. Swalen, D. L. Allara, J. D. Andrade, E. A. Chandross, S. Garoff, J. Israelachvili, T. J. McCarthy, R. Murray, R. F. Pease, J. F. Rabolt, K. J. Wynne, and H. Yu, "Molecular monolayers and films," Langmuir **3,** 932–950 (1987).
2. M. Lösche, "Protein monolayers at interfaces," Curr. Opin. Solid State Mater. Sci. **2,** 546–556 (1997).
3. A. Ulman, *Characterization of Organic Thin Films* (Butterworth-Heinemann, Stoneham, UK, 1995).
4. C. Nicolini, "Supramolecular architecture and molecular bioelectronics," Thin Solid Films **285,** 1–5 (1996).
5. B. J. Ratner, "The engineering of biomaterials exhibiting recognition and specificity," J. Mol. Recog. **9,** 617–625 (1996).
6. M. A. Bos and J. M. Kleijn, "Determination of the orientation distribution of adsorbed fluorophores using TIRF. 2. Measurements on porphyrin and cytochrome-*c*," Biophys. J. **68,** 2573–2579 (1995).
7. P. H. Axelsen and M. J. Citra, "Orientational order determination by internal reflection infrared spectroscopy," Prog. Biophys. Mol. Biol. **66,** 227–253 (1996).
8. G. J. Simpson, S. G. Westerbuhr, and K. L. Rowlen, "Molecular orientation and angular distribution probed by angle-resolved absorbance and second harmonic generation," Anal. Chem. **72,** 887–898 (2000).
9. A. Tronin and J. K. Blasie, "Variable acquisition angle total internal reflection fluorescence: a new technique for orientation distribution studies of ultrathin films," Langmuir **17,** 3696–3703 (2001).
10. D. M. Cropek and P. W. Bohn, "Surface molecular orientations determined by electronic linear dichroism in optical waveguide structures," J. Phys. Chem. **94,** 6452–6457 (1990).
11. P. L. Edmiston, J. E. Lee, L. L. Wood, and S. S. Saavedra, "Dipole orientation distributions in Langmuir–Blodgett films by planar waveguide linear dichroism and fluorescence anisotropy," J. Phys. Chem. **100,** 775–784 (1996).
12. P. L. Edmiston, J. E. Lee, S. S. Cheng, and S. S. Saavedra, "Molecular orientation distributions in protein films. 1. Cytochrome *c* adsorbed to substrates of variable surface chemistry," J. Am. Chem. Soc. **119,** 560–570 (1997).
13. P. L. Edmiston and S. S. Saavedra, "Molecular orientation distributions in protein films. 4. A multilayer composed of yeast cytochrome *c* bound through an intermediate streptavidin layer to a planar supported phospholipid bilayer," J. Am. Chem. Soc. **120,** 1665–1671 (1998).
14. S. B. Mendes and S. S. Saavedra, "Comparative analysis of absorbance calculations for integrated optical waveguide configurations by use of the ray optics model and the electromagnetic wave theory," Appl. Opt. **39,** 612–621 (2000).
15. M. B. Pereira and F. Horowitz, "Simple polarimetric approach to direct measurement of the near-surface refractive index in graded-index films," Appl. Opt. **42,** 3268–3270 (2003).
16. H. Nishihara, M. Haruna, and T. Suhara, *Optical Integrated Circuits* (McGraw-Hill, New York, 1989).
17. D. R. Dunphy, S. B. Mendes, S. S. Saavedra, and N. R. Armstrong, "The electroactive integrated optical waveguide: ultrasensitive spectroelectrochemistry of submonolayer adsorbates," Anal. Chem. **69,** 3086–3094 (1997).
18. J. T. Bradshaw, S. B. Mendes, N. R. Armstrong, and S. S. Saavedra, "Broadband coupling into a single-mode, electroactive integrated optical waveguide for spectroelectrochemical analysis of surface-confined redox couples," Anal. Chem. **75,** 1080–1088 (2003).
19. H. Kogelnik, "Theory of optical waveguides," in *Guided-Wave Optoelectronics*, T. Tamir ed. (Springer-Verlag, Berlin, 1990), pp. 43–50.
20. J. T. Bradshaw, S. B. Mendes, and S. S. Saavedra, "A simplified broadband coupling approach applied to chemically robust sol-gel, planar integrated optical waveguides," Anal. Chem. **74,** 1751–1759 (2002).
21. L. Yang, S. S. Saavedra, N. R. Armstrong, and J. Hayes, "Fabrication and characterization of low-loss, sol-gel planar waveguides," Anal. Chem. **66,** 1254–1263 (1994).
22. S. S. Saavedra and W. M. Reichert, "Prism coupling into polymer integrated optical waveguides with liquid superstrates," Appl. Spectrosc. **44,** 1210–1217 (1990).
23. L. Li, M. Xu, G. I. Stegeman, and C. T. Seaton, "Fabrication of photoresist masks for submicrometer surface relief gratings," in *Integrated Optical Circuit Engineering V*, M. A. Mentzer, ed., Proc. SPIE **835,** 72–82 (1987).
24. R. P. Haugland, "Fluorescent and biotinylated dextrans," in *Handbook of Fluorescent Probes and Research Products*, 9th ed., J. Gregory and M. T. Z. Spence, eds. (Molecular Probes, Eugene, Ore., 2002), pp. 581–583.
25. S. Liu, T. M. Sisson, and D. F. O'Brien, "Synthesis and polymerization of heterobifunctional amphiphiles to cross-link supramolecular assemblies," Macromolecules **34,** 465–473 (2001).

26. E. Kalb, S. Frey, and L. K. Tamm, "Formation of supported planar bilayers by fusion of vesicles to supported phospholipid monolayers," Biochim. Biophys. Acta **1103,** 307–316 (1992).
27. Vesicle fusion is a well-known self-assembly technique. On adsorption at a hydrophilic substrate–buffer interface, fluid bilayer vesicles spontaneously fuse to produce an extended, continuous lipid bilayer. See, for example, Refs. 28 and 29.
28. E. Sackmann, "Supported membranes: scientific and practical applications," Science **271,** 43–48 (1996).
29. A. L. Plant, "Supported hybrid bilayer membranes as rugged cell membrane mimics," Langmuir **15,** 5128–5135 (1999).
30. I. Thormaehlen, J. Straub, and U. Grigull, "Refractive index of water and its dependence on wavelength, temperature, and density," J. Phys. Chem. Ref. Data **14,** 933–945 (1985).
31. M. N. Timbs and N. L. Thompson, "Slow rotational mobilities of antibodies and lipids associated with substrate-supported phospholipid monolayers as measured by polarized fluorescence photobleaching recovery," Biophys. J. **58,** 413–428 (1990).